Thermal influence on charge carrier transport in solar cells based on GaAs PN junctions

Juan Osses-Márquez and Williams R. Calderón-Muñoz[a)]
Department of Mechanical Engineering, University of Chile, Beauchef 850, Santiago, Chile

(Received 25 March 2014; accepted 2 October 2014; published online 15 October 2014)

The electron and hole one-dimensional transport in a solar cell based on a Gallium Arsenide (GaAs) PN junction and its dependency with electron and lattice temperatures are studied here. Electrons and heat transport are treated on an equal footing, and a cell operating at high temperatures using concentrators is considered. The equations of a two-temperature hydrodynamic model are written in terms of asymptotic expansions for the dependent variables with the electron Reynolds number as a perturbation parameter. The dependency of the electron and hole densities through the junction with the temperature is analyzed solving the steady-state model at low Reynolds numbers. Lattice temperature distribution throughout the device is obtained considering the change of kinetic energy of electrons due to interactions with the lattice and heat absorbed from sunlight. In terms of performance, higher values of power output are obtained with low lattice temperature and hot energy carriers. This modeling contributes to improve the design of heat exchange devices and thermal management strategies in photovoltaic technologies. [http://dx.doi.org/10.1063/1.4898080]

I. INTRODUCTION

The major challenges with solar cells are improving the efficiency and lifetime as well as reducing manufacturing and material costs. The exposure of a photovoltaic PN junction solar cell to high sunlight concentration causes the device to heat up, where hotspots can produce a lack of efficiency in a photovoltaic panel and can reduce its lifetime. The design of cooling systems is one of the main concerns in concentrating photovoltaic technologies.[1] The modeling of charge carrier transport throughout a PN junction can provide the operating conditions needed to improve the electron and hole current densities and, consequently, the efficiency of photovoltaic solar cells.

In terms of performance, conventional PN junction solar cells are limited to a maximum efficiency about 33% as defined by the Shockley-Queisser limit,[2] and about 47% of the incident power would turn into heat within the cell.[3] For a given direct-bandgap semiconductor, photons with energies smaller than the band gap energy will not be absorbed. On the other hand, photons with energies larger than the bandgap energy will be absorbed, and the excess of energy will be distributed in the form of kinetic energy among the photogenerated carriers, electron-hole pairs. Therefore, under an excess kinetic energy greater than the band gap energy (k_{BT}), electrons can have an initial temperature greater than the surrounding lattice (hot electrons). This initial electron temperature can be as high as 3000 K with the lattice temperature at 300 K. Since the effective mass of electrons is typically much smaller than the effective mass of holes, the electrons will cool more slowly than holes. The hot electron kinetic energy is usually dissipated as heat to the lattice using carrier-phonon scattering mechanisms. If electrons can be extracted without heat losses, the efficiency can be about 67%.[3,4]

The modeling of semiconductor PN junction solar cells has been based on a drift-diffusion model.[2,5–7] This model gives a reasonable understanding of the physical processes involved in a PN junction based on a depletion region approximation, that is, a region where the carrier concentrations (electrons and holes) are considered to be negligible compared to the doping concentrations (N_A and N_D). The drift-diffusion model has two assumptions that limit the conclusions for electron and hole flows: (1) electron and hole temperatures are always the same as the lattice temperature and (2) electron and hole populations each form a quasi thermal equilibrium with a characteristic Fermi level and temperature.[2] Both assumptions are fairly rough for real applications, since the electric current flowing through the semiconductor structure heats this structure.[2] Because of that a mathematical model that provides a more detailed understanding of the transport of electrons and holes through PN junctions will help strongly not only in the design of more efficient photovoltaic solar cells but also in the thermal management of these devices.

In semiconductor modeling, hydrodynamic models have been used to describe the electron transport and temperature distributions in devices such as field effect transistors.[8,9] These models have also been used in the stability analysis of electron flow to understand whether semiconductors can be used as a radiative source,[10–13] and recently to study the electron and hole transport in quantum wells.[14–16] Physical similarities with fluid flow have been found for electron flow in semiconductor devices by using hydrodynamic models.[17] From a thermal perspective, two-temperature models have been used to describe semiconductor and thermoelectric devices.[18,19] Hydrodynamic models permit to avoid details of the distribution of electrons and holes by providing a set of partial differential equations to describe the voltage, the

[a)]Electronic mail: wicalder@ing.uchile.cl

evolution of the electron and hole velocities, densities, and temperatures throughout the junction.

In this paper, a thermal analysis of the electrons and lattice through the junction using a one-dimensional two-temperature hydrodynamic model is presented. The dependency of charge carrier and lattice temperatures with power output is discussed for a solar cell based on a GaAs PN junction.

II. HYDRODYNAMIC MODELING AND PHYSICAL CONSIDERATIONS

A. Governing equations

Current is driven through the device, shown in Fig. 1, by a voltage difference, diffusion, generation, and recombination processes between the two contacts at $x^*=0$, L. The coordinate x^* is in the direction of the electron flow, and t^* is time. The one-dimensional two-temperature hydrodynamic equations for electron and hole flow in a PN junction solar cell include, Gauss's law in Eqs. (1a) and (1b); mass conservation equations for electrons and holes in Eqs. (1c) and (1d); momentum conservation equations for electrons and holes in Eqs. (1e) and (1f); and energy conservation equation for electrons and lattice in Eqs. (1g) and (1h). We consider thermal equilibrium among electrons and holes. Therefore, the electron and hole temperature distributions are imposed to be equals throughout the device, T_c^*. The changes of kinetic energy of electrons due to their interactions with the lattice and lattice thermal energy are described in Eqs. (1g) and (1h). The system of equations is

$$\frac{\partial^2 V^*}{\partial x^{*2}} = -\frac{e}{\epsilon_s}(p^* - n^* - N_A), \quad x^* < x_J^*, \tag{1a}$$

$$\frac{\partial^2 V^*}{\partial x^{*2}} = -\frac{e}{\epsilon_s}(p^* - n^* + N_D), \quad x^* > x_J^*, \tag{1b}$$

$$\frac{\partial n^*}{\partial t^*} + \frac{\partial (u_e^* n^*)}{\partial x^*} = (G_n^* - R_n^*), \tag{1c}$$

$$\frac{\partial p^*}{\partial t^*} + \frac{\partial (u_h^* p^*)}{\partial x^*} = (G_p^* - R_p^*), \tag{1d}$$

$$\frac{\partial u_e^*}{\partial t^*} + u_e^* \frac{\partial u_e^*}{\partial x^*} = \frac{e}{m_e}\frac{\partial V^*}{\partial x^*} - \frac{k_B}{m_e n^*}\frac{\partial (n^* T_c^*)}{\partial x^*} - \frac{u_e^*}{\tau_{el}}, \tag{1e}$$

$$\frac{\partial u_h^*}{\partial t^*} + u_h^* \frac{\partial u_h^*}{\partial x^*} = -\frac{e}{m_h}\frac{\partial V^*}{\partial x^*} - \frac{k_B}{m_h p^*}\frac{\partial (p^* T_c^*)}{\partial x^*} - \frac{u_h^*}{\tau_{hl}}, \tag{1f}$$

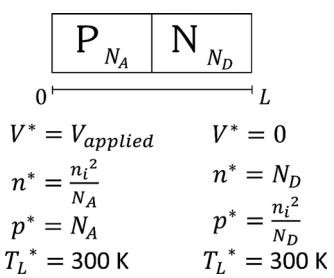

FIG. 1. Device scheme with boundary conditions.

$$\frac{\partial T_c^*}{\partial t^*} + u_e^* \frac{\partial T_c^*}{\partial x^*} = -\frac{2}{3} T_c^* \frac{\partial u_e^*}{\partial x^*} + \frac{2}{3n^* k_B}\frac{\partial}{\partial x^*}\left(k_e \frac{\partial T_c^*}{\partial x^*}\right) - \frac{T_c^* - T_L^*}{\tau_E} + \frac{m_e u_e^{*2}}{3k_B \tau_E} + \frac{2q_{heat}^*}{3n^* k_B}, \tag{1g}$$

$$C_L \frac{\partial T_L^*}{\partial t^*} = \frac{\partial}{\partial x^*}\left(k_L \frac{\partial T_L^*}{\partial x^*}\right) + \frac{3n^* k_B}{2}\left(\frac{T_c^* - T_L^*}{\tau_E}\right), \tag{1h}$$

where $V^*(x^*, t^*)$ is the electrostatic potential, $n^*(x^*, t^*)$ is the electron density, $p^*(x^*, t^*)$ is the hole density, $u_e^*(x^*, t^*)$ is the x^*-component electron drift velocity, $u_h^*(x^*, t^*)$ is the x^*-component hole drift velocity, T_c^* is the electron and hole temperature, T_L^* is the lattice temperature, and q_{heat}^* is an imposed heat per unit length in an unit area in which the current passes, which is absorbed from sunlight. The junction is defined at $x^* = x_J^*$.

The physical parameters are the electron charge, e, the permittivity of the semiconductor, ϵ_s, the donor concentration, N_D, the acceptor concentration, N_A, the effective electron mass, m_e, the effective hole mass, m_h, the Boltzmann constant, k_B, the generation rate for electrons, G_n^*, the generation rate for holes, G_p^*, the recombination rate for electrons, R_n^*, the recombination rate for holes, R_p^*, the momentum relaxation time for electrons, τ_{el}, the momentum relaxation time for holes, τ_{hl}, the energy relaxation time for electrons, τ_E, the lattice thermal conductivity k_L, and the heat capacity for lattice C_L. In this analysis, we consider τ_{el}, τ_{hl}, τ_E, k_L, and C_L as constant values. This description is an approximation and can be improved by introducing the maximum entropy principle of extended thermodynamics, where the collision terms are determined without the use of tunable parameters.[20]

The model considers only Shockley-Read-Hall recombination processes (SRH) for electrons and holes, since this mechanism determines the effective carrier lifetime. Therefore, the recombination rates depend exponentially on the applied voltage through the PN junction. The electric field, electron density, and hole density at both ends are prescribed boundary conditions. The physical realization is by considering heavily doped regions near the ends, which lead to ohmic contacts. Thus, the boundary conditions[21] are $\frac{dV^*}{dx^*}(0, t^*) = 0$, $\frac{dV^*}{dx^*}(L, t^*) = 0$ (at zero bias, zero total current density), $V^*(0, t^*) = V_{applied}$, $V(L, t^*) = 0$ (at applied bias), $n^*(0, t^*) = n_i^2/N_A$, $n^*(L, t^*) = N_D$, $p^*(0, t^*) = N_A$, and $p^*(L, t^*) = n_i^2/N_D$, where L is the length of the device and n_i is the intrinsic carrier concentration, which in this analysis we consider as a function of average lattice temperature. The boundary conditions for the lattice temperature are $T_L^*(0, t^*) = T_L^*(L, t^*) = 330$ K. The use of symmetric boundary conditions for the lattice temperature is supported by the fact that the results from thermal modeling of photovoltaic solar cells show that the temperature of the semiconductor layer is mostly uniform along the normal axis.[25] The device scheme with boundary conditions is shown in Fig. 1.

The charge carrier temperature distribution is imposed to be uniform in space and known throughout the device but it can be higher than the lattice and room temperatures, which can vary throughout the device. There are two reasons for this condition. First, carrier temperature fluctuations may

increase the recombination rate, reducing the PN junction performance,[22,23] and also, these fluctuations may modify the momentum and energy relaxation times more significantly throughout the device than fluctuations in the lattice temperature values.[24] Second, an operating condition determined by an imposed heat flux, q^*_{heat}, where the transport of hot electrons can be achieved and maintained through the device in order to reduce the lattice heating and, consequently, the recombination rates, improving the performance of the PN junction solar cell. By using $T^*_c = constant$ in space, Eqs. (1g) and (1h) can be written as follows:

$$C_L \frac{\partial T^*_L}{\partial t^*} = \frac{\partial}{\partial x^*}\left(k_L \frac{\partial T^*_L}{\partial x^*}\right) + \frac{1}{2\tau_E} m_e n^* u^{*2}_e + q^*_{heat} - n^* k_B T^*_c \frac{\partial u^*_e}{\partial x^*}. \quad (2)$$

By writing $V = V^*/V_0$, $n = n^*/N_0$, $p = p^*/N_0$, $x = x^*/L$, $u_e = u^*_e/U$, $u_h = u^*_h/U$, $T_c = T^*_c/T_0$, $T_L = T^*_L/T_0$, and $t = t^*U/L$, with V_0 is the reference voltage, N_0 is the reference doping density, T_0 is the reference temperature, and $q_0 = m_e N_0 U^2/\tau_{el}$ is the reference heat flux, the non-dimensional version of Eq. (1) is

$$\frac{\partial^2 V}{\partial x^2} = -\alpha\left(p - n - \frac{N_A}{N_0}\right), \quad x < x_J, \quad (3a)$$

$$\frac{\partial^2 V}{\partial x^2} = -\alpha\left(p - n + \frac{N_D}{N_0}\right), \quad x > x_J, \quad (3b)$$

$$\frac{\partial n}{\partial t} + \frac{\partial (u_e n)}{\partial x} = (G_n - R_n), \quad (3c)$$

$$\frac{\partial p}{\partial t} + \frac{\partial (u_h p)}{\partial x} = (G_p - R_p), \quad (3d)$$

$$R_e\left[\frac{\partial u_e}{\partial t} + u_e \frac{\partial u_e}{\partial x}\right] = \frac{\partial V}{\partial x} - \frac{\beta}{n}\frac{\partial n}{\partial x} - u_e, \quad (3e)$$

$$R_e\left[\frac{\partial u_h}{\partial t} + u_h \frac{\partial u_h}{\partial x}\right] = -m_r\left[\frac{\partial V}{\partial x} + \frac{\beta}{p}\frac{\partial p}{\partial x}\right] - \gamma u_h, \quad (3f)$$

$$\psi_1 \frac{\partial T_L}{\partial t} = \psi_2 \frac{\partial^2 T_L}{\partial x^2} + \frac{1}{2}\nu n {u_e}^2 + q_{heat} - \beta n \frac{\partial u_e}{\partial x}, \quad (3g)$$

where $\alpha = eL^2 N_0/V_0\epsilon_s$, $\gamma = \tau_{el}/\tau_{hl}$, $m_r = m_e/m_h$, $\beta = k_B T^*_c/eV_0$, $\nu = \tau_{el}/\tau_E$, $\psi_1 = \tau_{el} C_L T_0/m_e N_0 L U$, $\psi_2 = \tau_{el} k_L T_0/m_e N_0 L^2 U^2$, $R_e = U^2 m_e/eV_0$, $G_n - R_n = (G^*_n - R^*_n)L/N_0 U$, $G_p - R_p = (G^*_p - R^*_p)L/N_0 U$, and $U = eV_0 \tau_{el}/m_e L$ is the maximum average electron velocity. R_e is the Reynolds number and it can be written as $R_e = U\tau_{el}/L$, which is the Knudsen number for the electron cloud.

B. Mathematical and numerical methods

We consider the physical properties for GaAs shown in Table I, the system parameters shown in Table II, and the non-dimensional parameters shown in Table III. The values of the non-dimensional parameters have to be restricted to satisfy the built-in potential and the boundary conditions. The average time among collisions is small, and as a consequence, it is expected to have a small distance between two

TABLE I. Physical properties for GaAs.[9,19]

Constant	Value
e	1.60218×10^{-19} C
ϵ_s	113.28×10^{-12} C^2/(N m^2)
k_B	1.38066×10^{-23} J/K
k_L	42.61 W/(m K)
N_D	1×10^{16} m^{-3}
N_A	1×10^{16} m^{-3}
m_e	6.01×10^{-32} kg
m_h	4.65×10^{-31} kg
C_L	8.73×10^5 J/(m^3 K)
μ_{no}	0.45 m^2/(V s)
τ_p	2×10^{-12} s
τ_E	4.4×10^{-10} s

TABLE II. System parameters.

Constant	Value
L	840 μm
N_0	1×10^{16} m^{-3}
V_0	1.0 V
T_0	3000 K

TABLE III. Dimensionless parameters for GaAs.

Parameter	Value
α	10
γ	0.15
m_r	0.13
ν	0.0045
ψ_1	1.5×10^{12}
ψ_2	1.45×10^7
R_e	1.5×10^{-5}

collisions for an electron in the flow. This implies that the Reynolds number is small, $R_e < 1$, and it can be used as a perturbation parameter in asymptotic perturbation series[27] for the dependent variables in Eq. (3).

We are interested in the steady-state solution of Eq. (3). For the purposes of this paper, a symmetric PN junction in the dark and under light (constant net-generation rate), with $x_J = 0.5$ and $N_D = N_A$, was considered. Thus, the asymptotic perturbation series for the dependent variables are

$$\bar{V}(x) \approx \bar{V}_0(x) + \epsilon \bar{V}_1(x) + \cdots, \quad (4a)$$

$$\bar{n}(x) \approx \bar{n}_0(x) + \epsilon \bar{n}_1(x) + \cdots, \quad (4b)$$

$$\bar{p}(x) \approx \bar{p}_0(x) + \epsilon \bar{p}_1(x) + \cdots, \quad (4c)$$

$$\bar{u}_e(x) \approx \bar{u}_{e0}(x) + \epsilon \bar{u}_{e1}(x) + \cdots, \quad (4d)$$

$$\bar{u}_h(x) \approx \bar{u}_{h0}(x) + \epsilon \bar{u}_{h1}(x) + \cdots, \quad (4e)$$

where $\epsilon = R_e$. By replacing Eq. (4) into the steady-state version of Eq. (3), a zero order system is obtained. This system can be written in terms of electron and hole current densities. Two second order differential equations for the electron and hole current densities are obtained by combining the continuity and momentum conservation equations

$$\frac{d^2\bar{V}_0}{dx^2} = -\alpha\left(\bar{p}_0 - \bar{n}_0 - \frac{N_A}{N_0}\right), \quad x < x_J, \tag{5a}$$

$$\frac{d^2\bar{V}_0}{dx^2} = -\alpha\left(\bar{p}_0 - \bar{n}_0 + \frac{N_D}{N_0}\right), \quad x > x_J, \tag{5b}$$

$$\beta\frac{d^2\bar{n}_0}{dx^2} - \frac{d\bar{n}_0}{dx}\frac{d\bar{V}_0}{dx} - \bar{n}_0\frac{d^2\bar{V}_0}{dx^2} + (G_n - R_n) = 0, \tag{5c}$$

$$\beta\frac{d^2\bar{p}_0}{dx^2} + \frac{d\bar{p}_0}{dx}\frac{d\bar{V}_0}{dx} + \bar{p}_0\frac{d^2\bar{V}_0}{dx^2} + \frac{\gamma}{m_r}(G_p - R_p) = 0, \tag{5d}$$

where

$$\overline{u_e}_0 = \frac{d\bar{V}_0}{dx} - \frac{\beta}{\bar{n}_0}\frac{d\bar{n}_0}{dx}, \tag{6a}$$

$$\overline{u_h}_0 = -\frac{m_r}{\gamma}\left[\frac{d\bar{V}_0}{dx} + \frac{\beta}{\bar{p}_0}\frac{d\bar{p}_0}{dx}\right]. \tag{6b}$$

In the same way, the first order system is

$$\frac{d^2\bar{V}_1}{dx^2} = -\alpha(\bar{p}_1 - \bar{n}_1), \tag{7a}$$

$$\frac{d^2\bar{n}_1}{dx^2} + \frac{1}{\beta}\frac{d}{dx}\left(\bar{n}_0\bar{u}_{e0}\frac{d\bar{u}_{e0}}{dx}\right) - \frac{1}{\beta}\frac{d}{dx}\left(\bar{n}_1\frac{d\bar{V}_0}{dx}\right) - \frac{1}{\beta}\frac{d}{dx}\left(\bar{n}_0\frac{d\bar{V}_1}{dx}\right) = 0, \tag{7b}$$

$$\frac{d^2\bar{p}_1}{dx^2} + \frac{1}{m_r\beta}\frac{d}{dx}\left(\bar{p}_0\bar{u}_{h0}\frac{d\bar{u}_{h0}}{dx}\right) + \frac{1}{\beta}\frac{d}{dx}\left(\bar{p}_1\frac{d\bar{V}_0}{dx}\right) + \frac{1}{\beta}\frac{d}{dx}\left(\bar{p}_0\frac{d\bar{V}_1}{dx}\right) = 0, \tag{7c}$$

where

$$\overline{u_e}_1 = \frac{1}{\bar{n}_0}\left(-\bar{n}_1\bar{u}_{e_0} - \beta\frac{d\bar{n}_1}{dx} - \bar{n}_0\bar{u}_{e_0}\frac{d\bar{u}_{e_0}}{dx} + n_1\frac{d\bar{V}_0}{dx} - \bar{n}_0\frac{d\bar{V}_1}{dx}\right), \tag{8a}$$

$$\overline{u_h}_1 = \frac{1}{\gamma\bar{p}_0}\left(-\bar{p}_1\bar{u}_{h_0} - m_r\beta\frac{d\bar{n}_1}{dx} - \bar{p}_0\bar{u}_{h_0}\frac{d\bar{u}_{h_0}}{dx} - m_r\bar{p}_1\frac{d\bar{V}_0}{dx} - m_r\bar{p}_0\frac{d\bar{V}_1}{dx}\right). \tag{8b}$$

The lattice energy equation, Eq. (3g), is solved independently in the system of Eq. (3), by using the solutions of $\bar{n}(x)$ and $\bar{u}_e(x)$. A second order finite difference scheme was used to discretize the zero order model in Eq. (5) and the first order model in Eq. (7). A combined direct and iterative scheme was implemented in the software Mathematica to get the steady-state solution.

1. Relaxation time approximation

The collision terms in the momentum conservation equations and energy conservation equation for charge carriers are written using relaxation time approximations. The momentum relaxation times for electron and holes were assumed to have the values $\tau_{el} = 0.15\tau_p$ and $\tau_{hl} = \tau_p$. This assumption has two reasons; first, there are no scattering events between electrons and holes, and second, the parameter $\gamma = \tau_{el}/\tau_{hl}$ just affects the hole velocity values, as shown in Eqs. (6b) and (8b). Since the holes have a larger effective mass than electrons, it is expected that the hole velocity will be lower than the electron velocity and its contribution to the total current will be determined by the hole density. The energy relaxation time and momentum relaxation time were estimated by considering $T_L^* = 330\text{K}$ and $T_c^* = 3000\text{K}$ as reference values in Eq. (9) (Refs. 19 and 24)

$$\tau_p = \frac{m_e\mu_{no}}{e}\left(\frac{T_L^*}{T_c^*}\right), \tag{9a}$$

$$\tau_E = \frac{1}{2}\tau_p + \frac{3\mu_{no}k_BT_L^*}{2eU_s^2}\frac{T_c^*}{T_c^* + T_L^*}, \tag{9b}$$

where μ_{no} is the low-field mobility and $U_s = 10^5\,\text{m/s}$ is the saturation velocity.

2. Drift-diffusion model

In the neutral P and N regions, there are no electric fields,[6] that is, $d\bar{V}/dx = 0$. Equations (5c) and (5d) can be written as

$$\frac{d^2\bar{n}_0}{dx^2} + \frac{1}{\beta}(G_n - R_n) = 0, \tag{10a}$$

$$\frac{d^2\bar{p}_0}{dx^2} + \frac{\gamma}{m_r\beta}(G_p - R_p) = 0. \tag{10b}$$

By considering no generation process, $G_n = G_p = 0$, and the recombination process as $R_n = \bar{n}_0 - \bar{n}_{po}/\tau_{el}$ and $R_p = \bar{p}_0 - \bar{p}_{no}/\tau_{hl}$, where $\bar{n}_{po}$ is the electron concentration at equilibrium in the P-side, $\bar{p}_{no}$ is the hole concentration at equilibrium in the N-side of the junction, and applying $\bar{p}_n(x = \infty) = \bar{p}_{no}$, $\bar{n}_p(x = -\infty) = \bar{n}_{po}$ and the Shockley boundary conditions, the ideal diode equation can be obtained.[6] Therefore, with achievable assumptions the order zero solution of the hydrodynamic model used here is able to reproduce the well-known drift-diffusion model in PN junctions. This model assumes thermal equilibrium between lattice and charge carriers.

III. RESULTS AND DISCUSSION

A. Charge carrier transport and thermal effects

An example of non-dimensional values of electron density, $\bar{n}$, hole density, $\bar{p}$, electrostatic potential, $\bar{V}$ and electric field, $\bar{E}$, through a symmetric junction (in the dark, with no net-generation rate) is shown in Fig. 2. When β increases the thermal energy of electrons and holes increases with respect to a reference electron energy (eV_0). An operating condition of the device with higher charge carrier temperatures makes the electron and hole distributions smoother, the difference in electrostatic potential at both edges gets smaller and consequently, a lower maximum electric field. At zero-bias in the dark, the charge carrier temperatures and lattice temperature have the same value.

The applied bias defines an operating condition of the PN junction device. An example of non-dimensional values

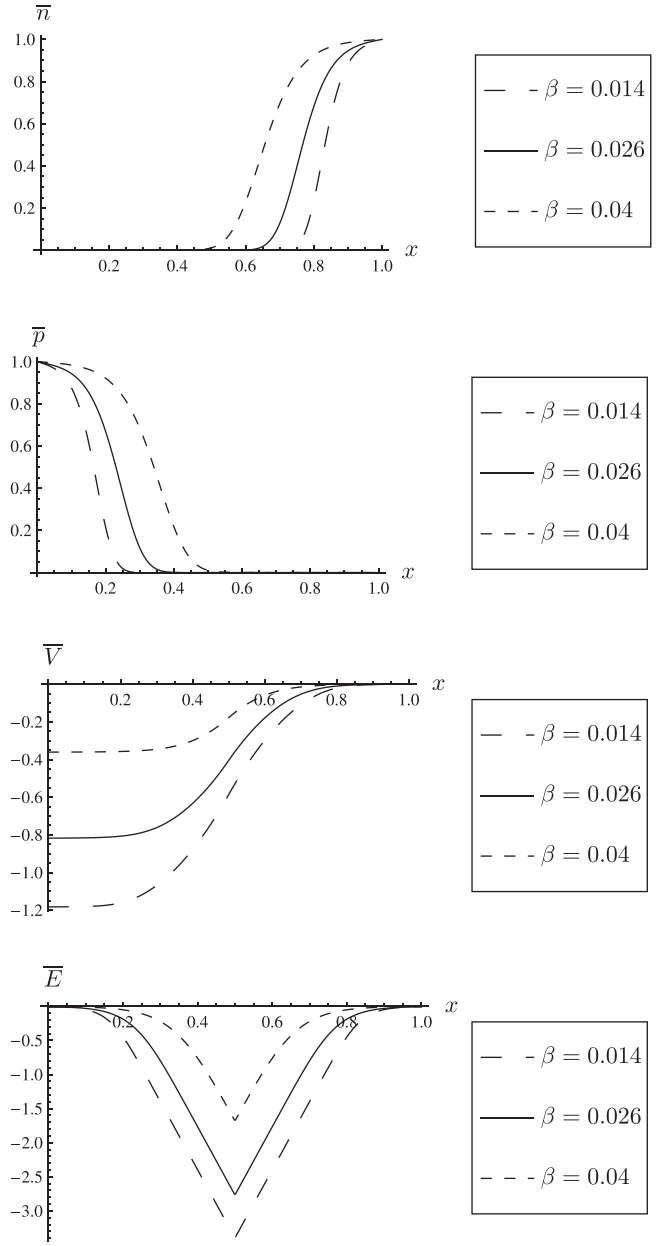

FIG. 2. Non-dimensional steady-state solution for a PN junction at zero-bias in the dark with $\alpha = 10$ and $R_e = 1.5 \times 10^{-5}$.

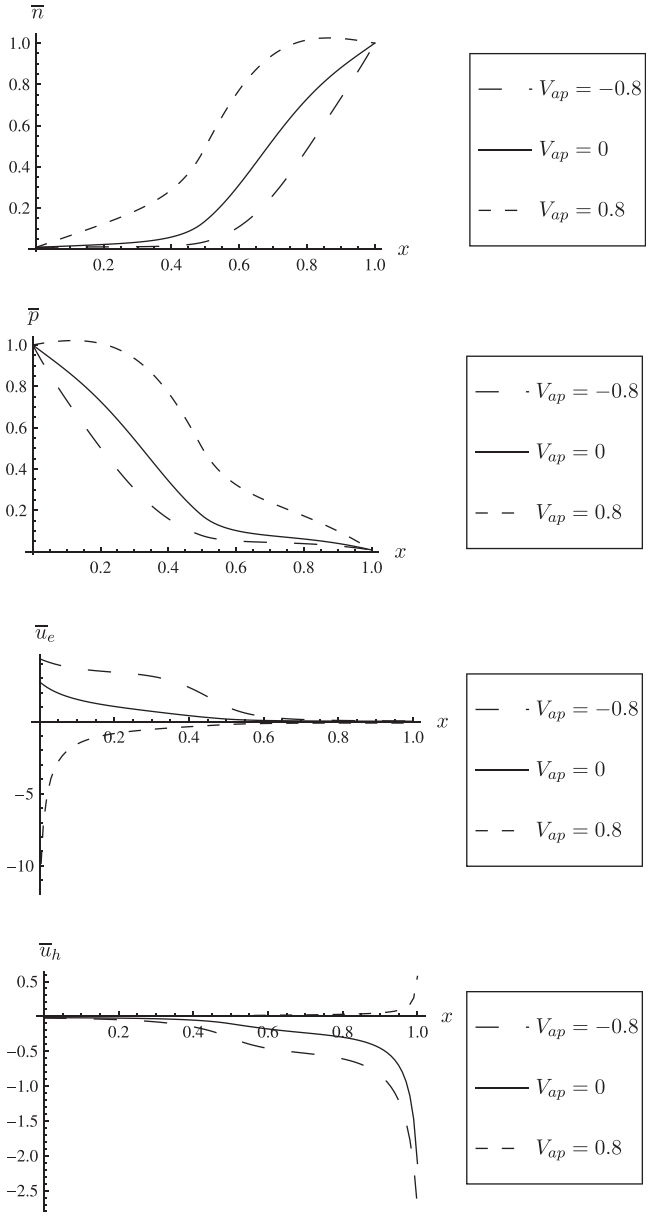

FIG. 3. Non-dimensional steady-state solution for a PN junction at forward, zero, and reverse bias under light with $\alpha = 10$, $R_e = 1.5 \times 10^{-5}$, $\beta = 0.25$, $T_L^* = 330$K (boundary conditions), and $G = 0.064$ (4.8×10^{15} 1/cm^{3}s).

of electron density, $\bar{n}$, hole density, $\bar{p}$, electron velocity, $\overline{u_e}$, and hole velocity, $\overline{u_h}$, through the junction is shown in Fig. 3. When the applied bias (V_{ap}) goes from reverse to forward, electron and hole densities increases throughout the junction device, and the absolute value of the electron velocity increases at the P-side edge and the hole velocity goes from negative to positive at the N-side. These results show how the total current density increases as the applied bias increases.

The influence of the charge carrier temperature in the charge transport is shown in Fig. 4. According to these results, when T_c decreases (β decreases), the absolute value of the electron velocity increases at the P-side edge, and the hole velocity changes more significantly in the region around the N-side edge. The lattice temperature, T_L^*, is a parabolic distribution throughout the device and reaches lower maximum values at lower values of T_c. The heat flux at both edges of the device is defined by the lattice thermal conductivity and the lattice temperature gradient. To have an operating condition with a lower value of T_c, the amount of heat that has to be released from both sides depends on the maximum value of T_L^* defined by boundary conditions and the desired value of T_c.

B. GaAs PN junction solar cell characteristics and comparison to experimental data

The voltage-current density characteristics in a GaAs PN junction solar cell with symmetric doping concentrations and sides, and with recombination and generation process were studied with the one-dimensional hydrodynamic model. The physical properties were obtained from Table I, with $N_0 = N_A = N_D = 1 \times 10^{21}\,\mathrm{m}^{-3}$, and the system parameters from Table II, with $L = 1.6\,\mu$m. Device length and doping

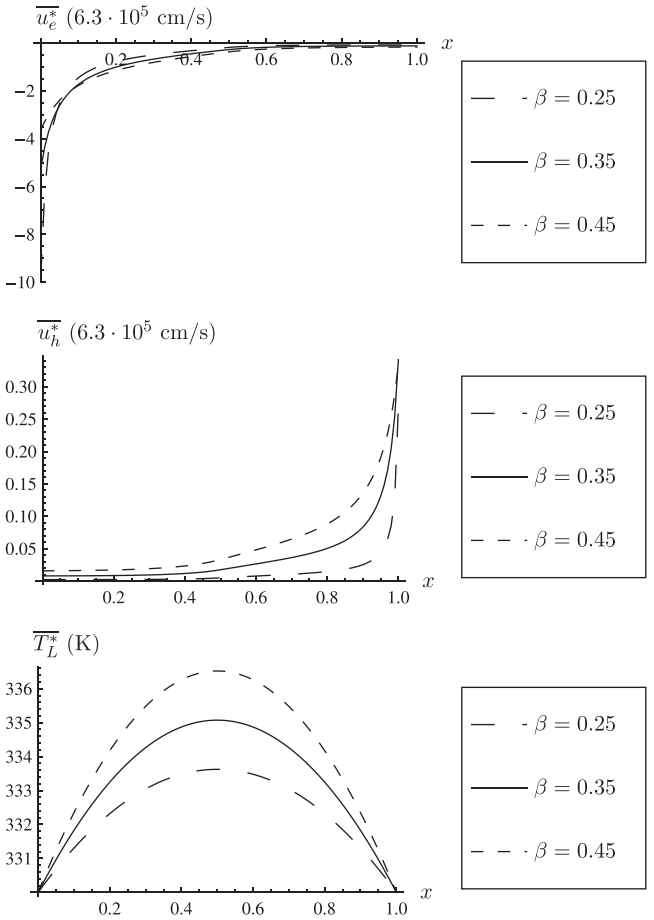

FIG. 4. Steady-state solution for a PN junction at forward bias under light with $\alpha = 10$, $R_e = 1.5 \times 10^{-5}$, $G = 0.064$ (4.8×10^{15} 1/cm^{3}s), $V_{ap}^* = 0.8$ (V), and $q_{heat} = 0.01$.

density are involved in the design of a PN junction, in particular, with applications to photovoltaic solar cells. These variables can define the size of the region where the most abrupt changes in carrier densities, electrostatic potential, and electric field distributions are taking place, and therefore, provide the information of the conduction and valence band bending in the region around the junction.

Examples of calculated voltage-current density characteristics are shown in Figs. 5 and 6. A good agreement between predicted by the model two-temperature hydrodynamic model and measured voltage-current characteristics is obtained when charge carrier temperature is higher than

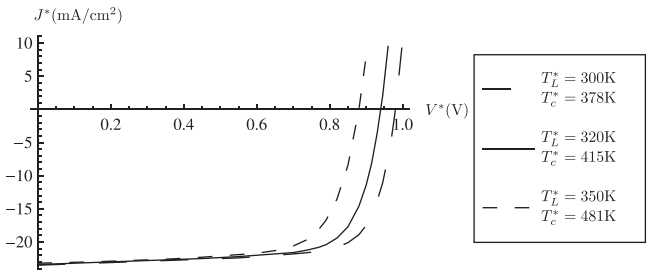

FIG. 5. Total current density-voltage characteristics for a GaAs PN junction solar cell under light with $\alpha = 3$, $R_e = 1.2 \times 10^{-2}$, 1 Sun, at different lattice temperature boundary conditions, T_L^*, and different charge carrier temperatures, T_c^*.

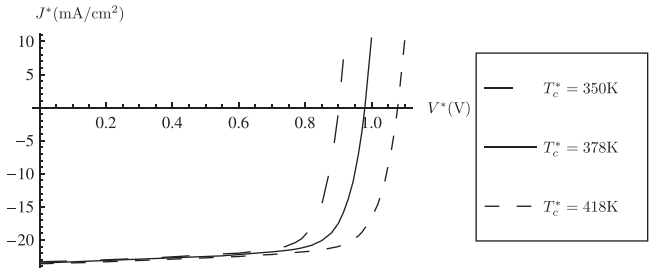

FIG. 6. Total current density-voltage characteristics for a GaAs PN junction solar cell under light with $\alpha = 3$, $R_e = 1.2 \times 10^{-2}$, 1 Sun, $T_L^* = 300$K (lattice temperature boundary conditions) at different charge carrier temperatures, T_c^*.

lattice temperature, as shown in Fig. 5. When the charge carriers heat up and the lattice temperature boundary conditions remain constant, the power output increases as shown in Fig. 6. This is in agreement with hot electron devices.[3,4] Small changes in the lattice temperature have a major influence in the power output values, as shown in Figs. 5 and 6. This can be explained by thermalisation losses in the junction. The open circuit voltage, V_{oc}, decreases and the short-circuit current, J_{sc}, increases when the cell temperature, T_L^*, increases.[28–30] The open-circuit voltage is in the order of 1 V at $T_L^* = 300$K, and increases when illumination intensity increases.[31] The predicted V_{oc} temperature coefficient is approximately -2 mV/°C as previously reported.[30,31]

C. Reynolds number and viscous effects

In order to investigate the effect of carrier temperatures, device length, and scattering effects in the total current densities through the junction, a PN junction with constant net-generation rates ($G^* = G_n^* - R_n^* = \text{constant}$) was studied. The non-dimensional generation and recombination rates can be written as $G_n - R_n = \alpha\eta(G_n^* - R_n^*)$ and $G_p - R_p = \alpha\eta(G_p^* - R_p^*)$, with $\eta = m_e\epsilon_s/N_0^2 e^2 \tau_{el}$. Therefore, variations in α can be considered to play a major role in variations of the non-dimensional net-generation rate $G = G_n - R_n = G_p - R_p$. In the one-dimensional hydrodynamic model, the non-dimensional number α takes into account the variations in device length. The Reynolds number R_e and η take into account the scattering effects through the momentum relaxation time for electrons τ_{el}. If the momentum relaxation time for electrons decreases at constant device length and net-generation rate, non-dimensional net-generation rate increases, therefore, total current increases. The Reynolds number can be written as $R_e = UL/(L^2/\tau_{el})$ where, in analogy with Fluid Mechanics, UL represents the inertial effects and (L^2/τ_{el}) represents the kinematic viscosity of the electron flow. By increasing the device length, L, (α increases) the viscous effects increases and diffusion of carriers is modified through the junction, the electron and hole distributions are smoother at both edges of the junction, the electrostatic potential distribution is smoother and the electric field distribution becomes sharper. In larger devices with a very short momentum relaxation time, most of the diffusion processes of carriers are taking place in a small region around the junction. This can contribute to the thermal diffusion and heat

dissipation at the edges of the device, in order to have lower carrier temperatures.

D. Improvements in design of concentrator solar cell

The power output of a concentrator solar cell can be increased by increasing the open circuit voltage, V_{oc}, and the short circuit current, J_{sc}, V_{oc}, and J_{sc} depend on operational conditions such as lattice temperature, charge carrier temperature, and light intensity as well as device characteristics such as device length and doping densities. The temperature characteristic of V_{oc} is influenced by the temperature characteristic of saturation current. This current is proportional to the square root of the ratio between the diffusion constant and lifetime of electrons, which ratio is usually represented by a power-law lattice temperature dependence, $T_L^{*\phi}$, with ϕ constant.[32] In the two-temperature hydrodynamic model, this ratio is proportional to the parameter β that corresponds to the non-dimensional electron thermal voltage ($\beta = 1$ represents $T_c^* \approx 11\,000$ K). Therefore, charge carrier temperature plays a fundamental role in the predicted value of V_{oc} and this suggests that some improvements can be done.

According to the results, when lattice temperature remains constant, V_{oc} increases with charge carrier temperature, as shown in Fig. 6. This can be achieve using contacts at both edges of the PN junction with a high electronic thermal conductivity in order to prevent charge carrier temperature fluctuations and avoid the heat dissipation of the photogenerated carriers into the lattice. On the other hand, lattice temperature boundary conditions are determined by lattice thermal conductivity as well as packaging layers in a PV module. Based on this analysis, the metal contacts and packaging layers have to be designed to dissipate the heat from hot charge carriers in a sufficiently large region away from the contact-semiconductor interface, in order to operate the solar cell at lower lattice temperatures.

IV. CONCLUSIONS

The electron and hole transport in a solar cell based on a GaAs PN junction was investigated using a one-dimensional two temperature hydrodynamic model. The results show that device length, charge carrier temperatures, applied bias, and lattice temperatures have an effect on the total current values changing the carrier distributions and velocities through the junction. These changes affect the current density-voltage characteristics by modifying the total current and slopes of the curves. A lower lattice temperature and higher charge carrier temperatures allow to increase the power output. Major changes in the charge carrier temperature imply small changes in the maximum lattice temperature. The presented modeling allows to study the thermal operating conditions of the PN junction, such as the lattice temperatures at the edges and the heat absorbed from sunlight, and their effects in the voltage-current density characteristics of the device. The prediction of lattice temperature distributions contributes to determine the PN junction thermal resistance and consequently, to design the thermal management strategies and heat exchangers to be used in photovoltaic modules.

ACKNOWLEDGMENTS

We are grateful to Debdeep Jena for valuable discussions and FONDECYT Project 11110235 (Chile) for financial support.

[1]A. Royne, C. J. Dey, and D. R. Mills, Sol. Energy Mater. Sol. Cells **86**, 451–483 (2005).
[2]J. Nelson, *The Physics of Solar Cells* (Imperial College Press, London, 2003).
[3]M. C. Beard and R. J. Ellingson, Laser Photonics Rev. **2**(5), 377–399 (2008).
[4]A. J. Nozik, Physica E **14**, 115–120 (2002).
[5]M. Shur, *Introduction to Electronic Devices* (John Wiley & Sons, Inc., New York, 1996).
[6]S. M. Sze, *Semiconductor Devices, Physics and Technology* (John Wiley & Sons, Inc., New York, 2002).
[7]A. S. Lin and J. D. Phillips, IEEE Trans. Electron Devices **56**, 3168–3174 (2009).
[8]K. Blotekjaer, IEEE Trans. Electron Devices **17**, 38–47 (1970).
[9]A. Majumdar, K. Fushinobu, and K. Hijikata, J. Appl. Phys. **77**, 6686–6694 (1995).
[10]M. Dyakonov and M. S. Shur, Phys. Rev. Lett. **71**, 2465–2468 (1993).
[11]M. Dyakonov and M. S. Shur, Appl. Phys. Lett. **87**, 111501 (2005).
[12]W. Calderón-Muñoz, M. Sen, and D. Jena, J. Appl. Phys. **102**, 023703 (2007).
[13]W. Calderón-Muñoz, D. Jena, and M. Sen, J. Appl. Phys. **106**, 014506 (2009).
[14]C. Y. Tsai, L. F. Eastman, and Y. H. Lo, Appl. Phys. Lett. **63**, 3408–3410 (1993).
[15]R. M. Abrarov, E. Y. Sherman, and J. E. Sipe, Appl. Phys. Lett. **91**, 232113 (2007).
[16]E. T. Sherman, R. M. Abrarov, and J. E. Sipe, J. Appl. Phys. **104**, 103701 (2008).
[17]K. Mohseni, A. Shakouri, R. J. Ranm, and M. C. Abraham, Phys. Fluids **17**, 100602 (2005).
[18]G. Chen, J. Appl. Phys. **97**, 083707 (2005).
[19]W. Calderón-Muñoz, D. Jena, and M. Sen, J. Appl. Phys. **107**, 074504 (2010).
[20]O. Muscato, V. Di Stefano, and C. Milazzo, J. Comput. Electron. **7**, 142–145 (2008).
[21]I. N. Volovichev, J. E. Velázquez-Pérez, and Yu. G. Gurevich, Sol. Energy Mater. Sol. Cells **93**, 6–10 (2009).
[22]I. N. Volovichev, G. N. Logvinov, O. Yu. Titov, and Yu. G. Gurevich, J. Appl. Phys. **95**, 4494–4496 (2004).
[23]S. Shishehchi, A. Asgari, and R. Kheradmand, Opt. Quantum Electron. **41**, 525–530 (2009).
[24]A. Jüngel and S. Tang, Appl. Numer. Math. **43**, 229–252 (2002).
[25]J. P. Kim, H. Lim, J. H. Song, Y. J. Chang, and C. H. Jeon, Sol. Energy Mater. Sol. Cells **95**, 404–407 (2011).
[26]G. M. M. W. Bissels, M. A. H. Asselbergs, G. J. Bauhuis, P. Mulder, E. J. Haverkamp, E. Vlieg, and J. J. Schermer, Sol. Energy Mater. Sol. Cells **104**, 97–101 (2012).
[27]M. H. Holmes, *Introduction to Perturbation Methods* (Springer, New York, 1995).
[28]G. S. Kinsey, P. Hebert, K. E. Barbour, D. D. Krut, H. L. Cotal, and R. A. Sherif, Prog. Photovoltaics: Res. Appl. **16**, 503–508 (2008).
[29]M. Y. Feteha and G. M. Eldallal, Renewable Energy **28**, 1097–1104 (2003).
[30]K. Nishioka, T. Takamoto, T. Agui, M. Kaneiwa, Y. Uraoka, and T. Fuyuki, Sol. Energy Mater. Sol. Cells **85**, 429–436 (2005).
[31]K. Nishioka, T. Takamoto, T. Agui, M. Kaneiwa, Y. Uraoka, and T. Fuyuki, Sol. Energy Mater. Sol. Cells **90**, 57–67 (2006).